SCIENCE ADVANCES | RESEARCH ARTICLE

CHEMISTRY

Gas-phase synthesis of anthracene and phenanthrene via radical-radical reaction induced ring expansions

Shane J. Goettl[1], **Andrew M. Turner**[1], **Vladislav S. Krasnoukhov**[2], **Valeriy N. Azyazov**[2], **Keisuke Kanayama**[3], **Patrick Hemberger**[3]*, **Alexander M. Mebel**[4]*, **Ralf I. Kaiser**[1]*

Unraveling reaction mechanisms of aromatic and resonance-stabilized radicals is critical to understanding molecular mass growth processes to polycyclic aromatic hydrocarbons (PAHs) and carbonaceous nanoparticles in distinct astrophysical environments (molecular clouds, circumstellar envelopes) and combustion systems. Using photoelectron photoion coincidence spectroscopy (PEPICO), we explored the gas-phase reaction of the methyl radical ($CH_3^{\bullet}$) with the aromatic and resonance-stabilized fluorenyl radical ($C_{13}H_9^{\bullet}$) under high-temperature conditions in a chemical microreactor. Anthracene and phenanthrene were detected isomer-selectively using photoionization efficiency (PIE) curves and mass-selected threshold photoelectron (ms-TPE) spectra. While phenanthrene is produced through a radical-radical recombination of the carbon-centered radicals, anthracene may plausibly be formed through an unconventional radical addition to a low spin-density fluorenyl carbon. These pathways result in five-membered ring expansion—a critical mechanism crucial to PAH mass growth converting bent PAHs into planar nanostructures.

INTRODUCTION

For the last decades, stable organic radicals have received extensive attention in the fields of synthetic organic chemistry and materials science for their use in molecular magnets (*1*), spintronics (*2*), batteries (*3*), and thermo- and optoelectronics (*4*–*6*). Resonance-stabilized free radicals (RSFRs) in particular—a class of organic open-shell species with multiple resonance contributors featuring an unpaired electron delocalized along the carbon backbone—are renowned for their stability and long lifetimes in the gas phase. Therefore, RSFRs are prevalent in interstellar and circumstellar environments (*7*–*14*) with simple RSFRs like propargyl ($C_3H_3^{\bullet}$) observed in cold molecular clouds at fractional abundances as high as 10^{-8} with respect to molecular hydrogen (*7*). RSFRs are also key growth species in bottom-up molecular mass growth processes to polycyclic aromatic hydrocarbons (PAHs) and carbonaceous nanomaterials in these astrophysical environments as well as in combustion systems (*15*). Recent investigations suggest reaction pathways to complex PAHs and eventually carbonaceous grains and soot particles initiated by small RSFRs such as propargyl ($C_3H_3^{\bullet}$), cyclopentadienyl ($C_5H_5^{\bullet}$), benzyl ($C_7H_7^{\bullet}$), 1-indenyl ($C_9H_7^{\bullet}$), and 1-/2-methylnaphthyl ($C_{11}H_9^{\bullet}$) (*15*–*19*). In deep space (*20*–*23*), PAHs and their derivatives have been detected in carbonaceous chondrites such as Allende, Murchison, and Orgueil (*24*–*26*), and recently in asteroids, as evidenced by the return samples from the Hayabusa2 mission to Ryugu (*27*). Sophisticated ^{13}C analyses of these samples disclosed at least two distinct environments for PAH formation including high-temperature regions, e.g., circumstellar envelopes of carbon-rich stars and planetary nebulae, and low-temperature regions such as cold molecular clouds. In the Taurus Molecular Cloud (TMC-1), for example, substituted PAHs of up to four benzene rings (*28*, *29*), as well as those incorporating a five-membered ring (*30*–*32*), have recently been observed using microwave spectroscopy with substituted aromatics likely formed through barrierless reactions of cyano radicals (CN) with aromatic molecules like benzene (C_6H_6) as demonstrated in crossed molecular beam experiments (*33*, *34*) validated by modeling (*35*). Yet, a critical divergence between astronomical observations and astrochemical models still persists, with predicted PAH lifetimes in the interstellar medium (ISM) an order of magnitude lower than the expected timescale of PAH injection from circumstellar envelopes and planetary nebulae (*36*–*38*). These findings reveal that critical molecular mass growth processes to aromatic matter in deep space are lacking.

RSFRs have been contemplated in bridging this gap between our understanding of molecular mass growth processes to aromatics in space in conjunction with astrochemical models and the reality of astronomical observations (*39*). Nevertheless, a thorough experimental investigation of the reactivity of multi-ringed, i.e., three- or four-membered, RSFRs and their role in the gas phase formation of aromatics is in its infancy predominantly due to previously insurmountable experimental difficulties in preparing clean radical sources of heavy RSFRs. Particular attention focuses on unconventional reaction mechanisms beyond a recombination of two radicals at their classical radical centers. Here, we report on a combined experimental and computational exploration of the radical-radical reaction of fluorenyl ($C_{11}H_9^{\bullet}$) with methyl ($CH_3^{\bullet}$) in the gas phase using a high-temperature chemical microreactor and velocity map imaging (VMI) photoelectron photoion coincidence spectroscopy (PEPICO). Products were preserved in a molecular beam, and photoionization with synchrotron vacuum ultraviolet (VUV) light led to isomer-selective identification of two $C_{14}H_{10}$ isomers phenanthrene and anthracene using photoionization efficiency (PIE) curves and photoion mass-selected threshold photoelectron (ms-TPE) spectra. Two distinct reaction mechanisms were unraveled arising from the unique resonance structures of the fluorenyl radical. While the phenanthrene isomer is accessed through a typical radical-radical recombination in the entrance channel from the methyl attack to the C9 carbon-centered fluorenyl radical, the gas phase preparation of

---

[1] Department of Chemistry, University of Hawai'i at Mānoa, Honolulu, HI 96822, USA. [2] Samara National Research University, Samara 443086, Russian Federation. [3] Paul Scherrer Institute, CH-5232 Villigen PSI, Switzerland. [4] Department of Chemistry and Biochemistry, Florida International University, Miami, FL 33199, USA.
*Corresponding author. Email: patrick.hemberger@psi.ch (P.H.); mebela@fiu.edu (A.M.M.); ralfk@hawaii.edu (R.I.K.)

anthracene may plausibly commence with an unexpected backside union between the methyl radical center and the C4a carbon atom of fluorenyl—a pathway that is classically not allowed in reactions between two carbon-centered radicals. Observation of this pathway offers critical insight into the unusual reactivity of RSFRs and reinforces the necessity of searching for versatile reaction mechanisms against conventional knowledge crucial to molecular mass growth processes in extreme environments while also demonstrating the importance of five-membered ring expansion reactions through its methylation toward the high-temperature formation of carbonaceous nanoparticles, which was recently demonstrated to be an integral part of PAH growth using kinetic Monte Carlo simulations (*40*).

RESULTS

Mass spectra

Photoionization mass spectra were collected for the reaction of methyl [$CH_3^•$, 15 atomic mass units (amu)] with fluorenyl ($C_{13}H_9^•$, 165 amu) at a photon energy of 9.00 eV and reactor temperature of 1700 ± 100 K (Fig. 1), where the radicals were generated from acetone (CH_3COCH_3) and 9-bromofluorene ($C_{13}H_9Br$), respectively. A blank experiment in which the acetone/helium reactant gas mixture was replaced by pure helium is shown in Fig. 1A, while Fig. 1B displays the data for the acetone/9-bromofluorene system. In both cases, ion counts were observed for mass-to-charge ratios (m/z) of 165 ($C_{13}H_9^+$), 166 ($^{13}CC_{12}H_9^+$, $C_{13}H_{10}^+$), 244 ($C_{13}H_9{}^{79}Br^+$), and 246 ($C_{13}H_9{}^{81}Br^+$). The latter two peaks originate from the ^{79}Br and ^{81}Br isotopes of the 9-bromofluorene precursors, respectively, while the former two are due to the fluorenyl radical (165 amu) and the naturally occurring ^{13}C-substituted fluorenyl radical (166 amu) accounting for the 1.1% natural abundance of ^{13}C. Note that the relative intensity of the $m/z = 166$ peak compared to that at $m/z = 165$ for the acetone/9-bromofluorene spectrum is far greater than for the helium/9-bromofluorene case. The larger signal is likely due to the formation of 9*H*-fluorene ($C_{13}H_{10}$) from recombination of the fluorenyl radical with a hydrogen atom (fig. S3), where the additional hydrogen atoms could arise from the acetone reactant. The acetone/9-bromofluorene system features additional peaks at $m/z = 167$ ($^{13}CC_{12}H_{10}^+$), 176 ($C_{14}H_8^+$), 178 ($C_{14}H_{10}^+$), 179 ($^{13}CC_{13}H_{10}^+$), 180 ($C_{14}H_{12}^+$), and 184 ($C_{14}H_{16}^+$), which were not observed in the blank experiment. Signal at $m/z = 167$ is likely due to ^{13}C-substituted 9*H*-fluorene, $m/z = 176$ may come from successive dehydrogenation of higher mass products ($m/z = 178$, 179), $m/z = 180$ could be caused by methylfluorene isomers from radical recombination/addition of methyl with fluorenyl (fig. S3), and $m/z = 184$ is possibly a product of successive hydrogenation of lower mass products. Finally, peaks at $m/z = 178$ and 179 provide evidence for the formation of $C_{14}H_{10}$ isomer(s) and their ^{13}C-substituted counterpart(s) from the reaction of the methyl radical with the fluorenyl radical.

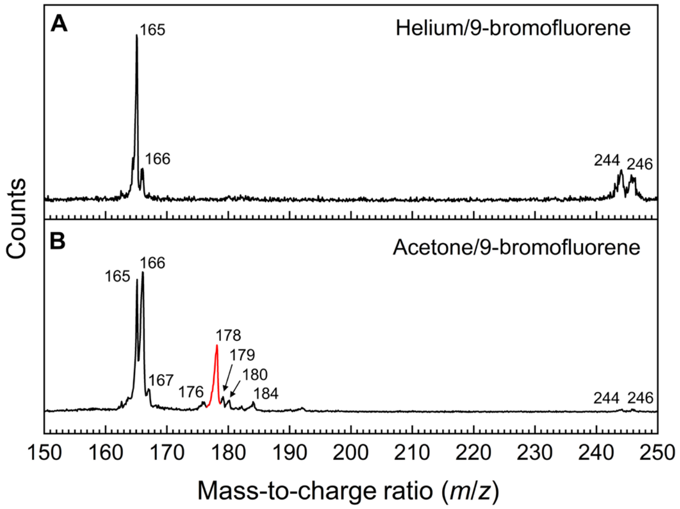

Fig. 1. Photoionization mass spectra. Comparison of mass spectra taken at a photon energy of 9.00 eV for the helium (He)–9-bromofluorene ($C_{13}H_9Br$) (**A**) and acetone (C_3H_6O)–9-bromofluorene ($C_{13}H_9Br$) (**B**) systems at a reactor temperature of 1700 ± 100 K. The mass peak of the newly formed $C_{14}H_{10}$ ($m/z = 178$) species is highlighted in red.

PIE curves

With the detection of $C_{14}H_{10}$ isomer(s) from the methyl-fluorenyl reaction, additional analytical techniques are required to obtain isomer-specific structural information on the formed products. Here, PIE curves and ms-TPE spectra were used to identify the specific species observed. PIE curves depict the ion counts versus the photon energy at a specific m/z, whereas ms-TPE spectra select only photoions at the desired m/z in coincidence with the threshold photoelectrons having kinetic energy less than 10 meV. First, PIE curves were collected at $m/z = 178$ ($C_{14}H_{10}^+$) in a photon energy range of 7.00 to 9.00 eV in 0.02-eV steps (Fig. 2A). The experimentally derived PIE curve features an ionization onset of 7.40 ± 0.05 eV, which is well matched by a reference PIE onset for anthracene of 7.38 ± 0.01 (*41*). However, at photon energies above 7.70 eV, the anthracene spectrum alone cannot account for the intensity observed in the experiment; therefore, additional contribution(s) are needed. Incorporating the reference PIE curve for phenanthrene (*42*) provides an excellent match for the higher photon energy portion of the experimental PIE such that a linear combination of both anthracene and phenanthrene offers a reasonable fit of the whole experimental spectrum. Note that the phenanthrene PIE exhibits an ionization onset of 7.85 ± 0.01 eV and therefore cannot replicate the experimental PIE alone. Using the absolute ion counts and photoionization cross sections of 16.7 ± 0.9 and 17.2 ± 0.9 Mb for anthracene and phenanthrene at 9.00 eV (*43*), the branching ratio between the two can be calculated, giving values of 17 ± 5% and 83 ± 5%, respectively.

ms-TPE spectra

Additional insight on the reaction products can be obtained through analysis of the ms-TPE spectra (Fig. 2B), which were also collected with the same parameters as the PIE curves. The experimental ms-TPE spectra feature distinct peaks at 7.42, 7.60 (with a shoulder at 7.64), and 7.76 ± 0.02 eV. The positioning of these features coincide with the origin $\left(0_0^0\right)$, C–C trans-annular stretching $\left(3_0^1\right)$, C–C in-plane symmetric stretching $\left(1_0^1\right)$, and overtone $\left(3_0^2\right)$ vibronic transitions, respectively, of anthracene (*41*, *44*). However, relative intensities of these peaks do not fully support this assignment, as the 7.42-, 7.60-, and 7.76-eV peaks all feature similar intensities. This is also contrary to the computed Franck-Condon (FC) factors for the 3_0^1, 1_0^1, and 3_0^2 vibronic transitions for anthracene, which are more than an order of magnitude lower than that for the origin, which speaks for the contribution of another isomer. Thus, we searched for $C_{14}H_{10}$

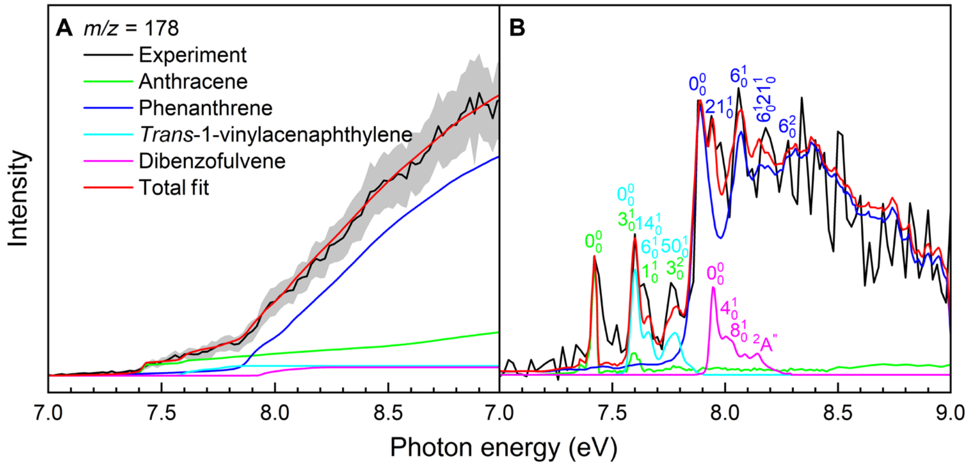

Fig. 2. PIE curves and ms-TPE spectra. PIE curves (**A**) and ms-TPE spectra (**B**) taken at m/z = 178 ($C_{14}H_{10}$) at a reactor temperature of 1700 ± 100 K. Black, acetone (C_3H_6O)–9-bromofluorene ($C_{13}H_9Br$) experimental spectra; blue, phenanthrene reference spectra from Rouillé *et al.* (*42*); green, anthracene reference spectra from Mayer *et al.* (*41*); cyan, *trans*-1-vinylacenaphthylene calculated spectra; magenta, dibenzofulvene calculated spectra; red, total fit obtained by summing the individual curves in each frame. Vibronic transitions for anthracene and phenanthrene were obtained from Sattasathuchana *et al.* (*44*), and the remaining were calculated in this work. The overall error bars (gray area) consist of two parts: 1σ error of the PIE curve averaged over the individual scans and ±10% based on the accuracy of the photodiode.

isomers and found that the shouldered 7.60- and 7.78-eV transitions might be described by *trans*-1-vinylacenaphthylene (Fig. 2B) with 6_0^1 and 14_0^1 vibrational transitions, assigned to a C–C–C bending mode at the vinyl moiety and a ring breathing mode of the five-membered ring, respectively. The band at around 7.78 eV is mostly associated with an excitation of the 50_0^1 mode, another five-ring deformation vibration. The CBS-QB3 calculated adiabatic ionization energy (AIE) of 7.61 eV fits exactly with the position of the 0–0 transition around 7.60 eV, while *trans*-1-vinylacenaphthylene is around 116 kJ mol^{-1} (CBS-QB3) less stable than phenanthrene (vide infra). The band at 7.60 eV may also be associated with *cis*-1-vinylacenaphthylene [AIE calculated with CBS-QB3 ($\mathrm{AIE_{CBS\text{-}QB3}}$) = 7.68 eV] and the three fulvenylnaphthalene isomers, which have calculated AIEs in the 7.55- to 7.61-eV energy range and very similar FC simulated spectra (fig. S5), reproducing both bands at 7.60 and 7.78 eV well. All isomers are around 1.2 eV less stable than phenanthrene, making them all viable candidates for a spectral assignment (vide infra).

Additionally, the experimental ms-TPE spectra have a high-intensity broad feature spanning from about 7.8 to 9.0 eV, which cannot be accounted for by the previously discussed isomers. Using the reference ms-TPE spectra of phenanthrene (*42*), the experimental peaks at 7.88 ± 0.02 and 8.06 ± 0.02 eV are matched very well with the origin $\left(0_0^0\right)$ and C–C stretching $\left(6_0^1\right)$ transitions of phenanthrene (*44*) while also agreeing with the spectral trend onward to 9.0 eV. Note that the $C_{14}H_{10}$ isomer dibenzofulvene may also contribute to the experimental spectrum in the 7.9 to 8.2 eV range as shown by the calculated FC spectrum of dibenzofulvene, where the origin band of dibenzofulvene matches the experimental shoulder at 7.94 ± 0.02 eV (Fig. 2B). Overall, the PIE curves and ms-TPE spectra provide convincing evidence for the production of at least anthracene and phenanthrene—and possibly dibenzofulvene and a combination of *cis*-/*trans*-1-vinylacenaphthylene, 1-/3-fulvenyl[*a*]naphthalene, and 1-fulvenyl[*b*]naphthalene (fig. S5)—from the reaction of the methyl radical with the fluorenyl radical. PIE curves and ms-TPE spectra of detected species at other mass channels are shown in figs. S1 to S3.

Potential energy surface

To elucidate the formation mechanisms of the observed products from the methyl-fluorenyl radical-radical reaction, we complement the experimental results with electronic structure calculations (Figs. 3 and 4). While the fluorenyl radical features multiple resonance contributors (*45*), the majority of the spin density is located on the C9 carbon, i.e., the point of the five-membered ring not included in the six-membered rings (Fig. 5); therefore, the C9 carbon can be considered the classical fluorenyl radical center. As expected, based on textbook radical-radical reactions, the reaction is initiated by the barrierless recombination of the radical sites in the methyl and fluorenyl radicals through carbon-carbon single bond coupling, forming the 9-methylfluorenyl molecule (**i1**) stabilized by 298 kJ mol^{-1} with respect to the separated reactants. The barrierless formation of **i1** from the reactants is verified by the potential energy scan along the minimal energy path (MEP) illustrated in fig. S6A. From here, **i1** undergoes atomic hydrogen loss to the 9-methyl-9-fluorenyl radical (**i2**) without barrier, followed by [1,2]-H shift from the methyl group to the five-membered ring over a large 212 kJ mol^{-1} barrier to **i3**. Both **i2** and **i3** can lose a hydrogen through unimolecular decomposition to dibenzofulvene (**p3**) through rather loose exit transition states of 4 and 26 kJ mol^{-1} above **p3**, respectively, in overall endoergic reactions. Alternatively, isomerization processes may continue from **i3**, starting with three-membered ring closure (**i3** → **i4**) followed by the five-membered ring opening up to a six-membered ring (**i4** → **i5**) before eventual hydrogen atom loss forming phenanthrene (**p1**). Comparing the branching point from **i2**, the barriers from **i2** → **p3** versus **i2** → **i3** are similar; therefore, both phenanthrene and dibenzofulvene are expected to form, whereas the entropic factor favors the formation of the latter. Dibenzofulvene can be rapidly converted to the thermodynamically more stable phenanthrene via hydrogen atom–assisted isomerization featuring a rather low barrier of 9 to 26 kJ mol^{-1}. As inclusion of the dibenzofulvene ms-TPE spectra causes a better fit of the experimental spectrum, we conclude that dibenzofulvene is likely forming and at least some of this isomer remains after any decomposition or isomerization pathways.

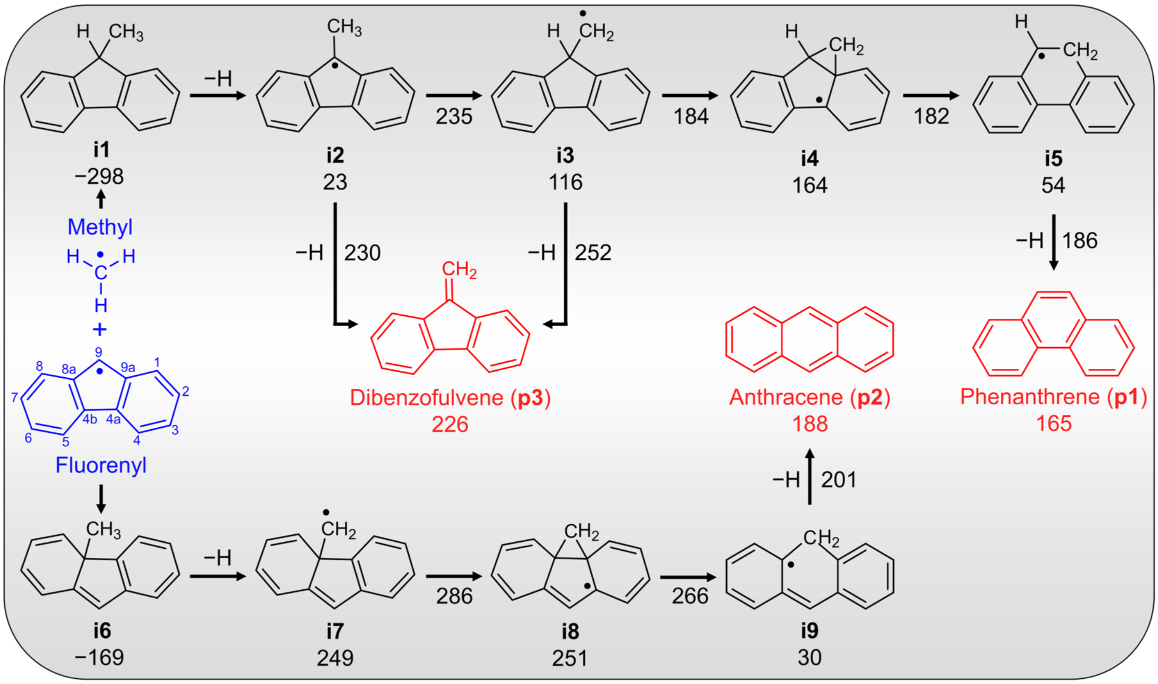

Fig. 3. Potential energy diagram of reaction pathways to p1 to p3. Schematic potential energy diagram for the reaction of the methyl radical (CH_3) with the fluorenyl radical ($C_{13}H_9$) calculated at the G3(MP2,CC)//ωB97XD/6-311G** level of theory. Reactants are shown in blue, intermediates are black, products are red, and relative energies are in kJ mol^{-1}. The full scheme is shown in fig. S4.

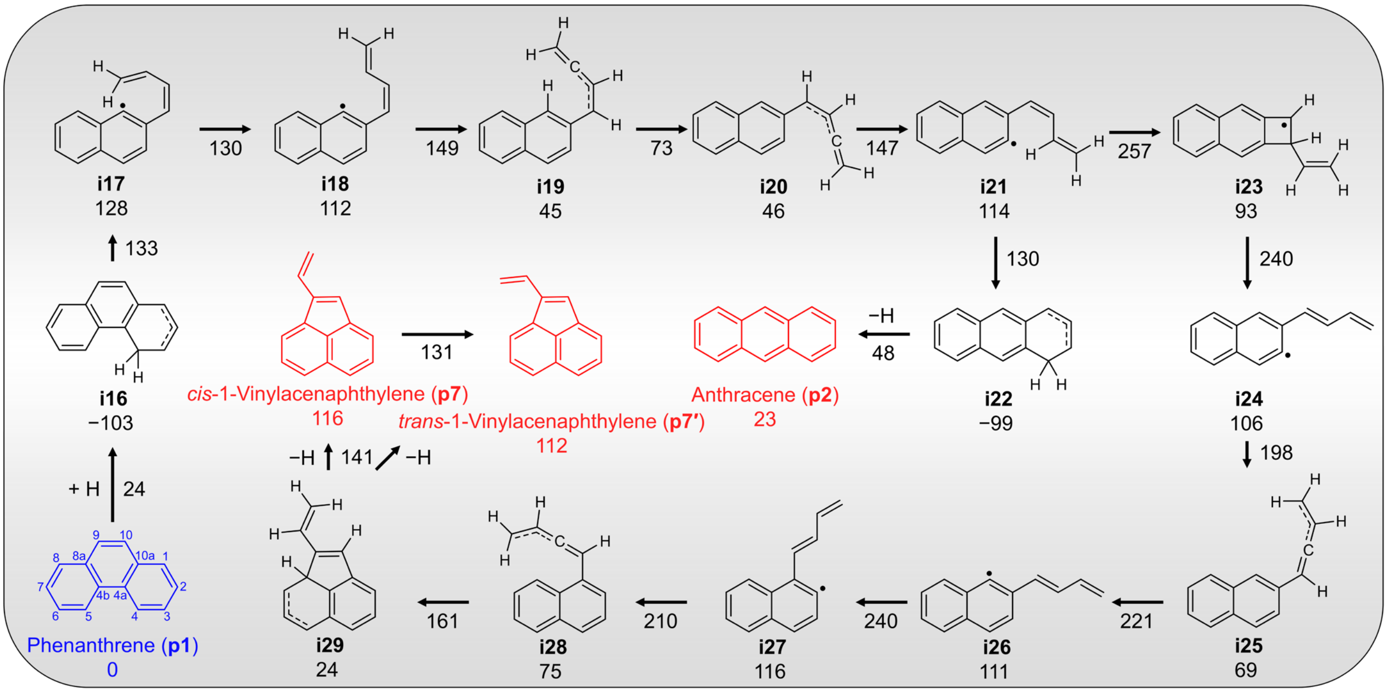

Fig. 4. Potential energy diagram starting from phenanthrene. Schematic potential energy diagram for H-assisted isomerization of phenanthrene (**p1**), which was previously partially investigated by Zhao *et al.* (*46*). Reactants are shown in blue, intermediates are black, products are red, and relative energies are in kJ mol^{-1}.

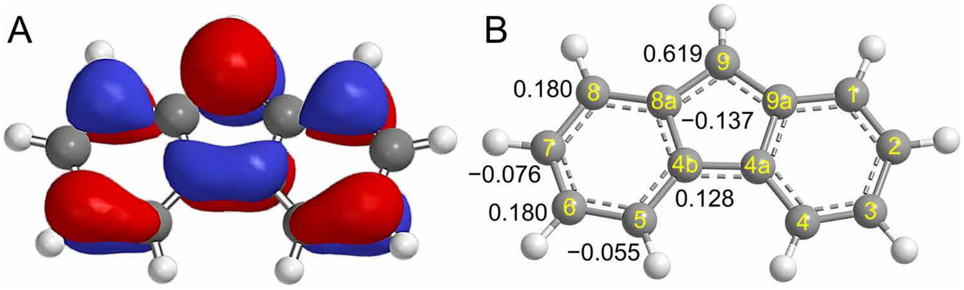

Fig. 5. Fluorenyl radical structure. Singly occupied highest occupied molecular orbital (HOMO) (**A**) and electron spin density distribution (**B**) calculated for the fluorenyl radical ($C_{13}H_9$).

While phenanthrene constitutes the major product contribution from the methyl-fluorenyl system, the experiments also identify anthracene (**p2**). The conventional radical center recombination between the methyl radical and C9 carbon of fluorenyl cannot lead to **p2**, so there must be alternate reaction route(s). Other carbon atoms in the fluorenyl radical feature spin densities with absolute values ranging from 0.055 to 0.180 *e*, in the best case over three times lower than the C9 spin density of 0.619 *e* (Fig. 5). Further, methyl addition to the C1 or C3 carbons of fluorenyl—those with the highest spin densities aside from C9—would not lead to anthracene, likely producing benz[a]azulene (**p4,** $AIE_{CBS\text{-}QB3}$ = 7.07 eV) or 1-/3-methylidenefluorene (**p5**, $AIE_{CBS\text{-}QB3}$ = 7.35 eV/**p6**, $AIE_{CBS\text{-}QB3}$ = 6.96 eV) instead. These isomers were not observed experimentally and are not energetically favorable, the pathways to each displaying barriers of over 300 kJ mol^{-1} with respect to reactants (fig. S4). A pathway that can produce anthracene is initiated by barrierless methyl radical addition to the C4a carbon of fluorenyl (Fig. 3), which has a spin density of only 0.128 *e* (Fig. 5). Nevertheless, considering the spin density distribution and resonance structures of the fluorenyl radical, this interaction constitutes a unique entrance channel featuring radical-radical recombination of the methyl radical with the C4a carbon of fluorenyl forming 4a-methylfluorene (**i6**) at 169 kJ mol^{-1} below the separated reactants. Again, the barrierless character of the $CH_3^{\bullet} + C_{13}H_9^{\bullet} \rightarrow$ **i6** pathway has been confirmed by the computed MEP (fig. S6B). This reaction route continues with atomic hydrogen loss from the methyl group (**i6** → **i7**), three-membered ring closure (**i7** → **i8**), five-membered ring opening up to a six-membered ring (**i8** → **i9**), and finally unimolecular decomposition via hydrogen atom loss to anthracene (**p2**). Considering the highest barrier in the phenanthrene formation route of 235 kJ mol^{-1} with respect to the separated reactants (**i2** → **i3**), the reaction sequence to anthracene is less favorable not only with regard to the radical-radical recombination site (C9 versus C4a) but also from an energetics standpoint, as the rate-controlling transition state (**i7** → **i8**) is about 50 kJ mol^{-1} higher than is the case for the phenanthrene pathway. As such, the low experimental branching ratio of anthracene compared to phenanthrene is expected.

An alternative source of anthracene, along with 1-vinylacenaphthylene (**p7/p7′**), could be hydrogen-assisted isomerization of phenanthrene [Fig. 4, note that a part of this potential energy surface (PES) was explored in a previous work on the reactions of naphthyl radicals with vinylacetylene (*46*)]. Along the path to anthracene, one of the six-membered rings of phenanthrene opens after an H atom addition (**p1** → **i16** → **i17**), which is followed by rotations of the C_4H_{4-5} side chain and facile hydrogen atom migrations to and from this side chain and the neighboring ring (**i17** → **i18** → **i19** → **i20** → **i21**), and finally ring re-closure and elimination of the extra hydrogen atom (**i21** → **i22** → **p2**). The highest energy transition state along this pathway lies 149 kJ mol^{-1} above the phenanthrene plus atomic hydrogen reactants and corresponds to a hydrogen migration step (**i18** → **i19**). An alternative route from **i21** involves a four-membered ring opening and closure, resulting in a *cis-trans* isomerization of the C_4H_5 side chain followed by rotations and H shifts eventually leading to **i28**. The latter then undergoes a five-membered ring closure to **i29** and atomic hydrogen elimination producing 1-vinylacenaphthylene (**p7/p7′**). Although the pathway from **p1** to **p7** is mechanistically feasible, it features the highest barrier of 257 kJ mol^{-1} relative to **p1** + H for the **i21** → **i23** step and, hence, is expected to be less competitive than the secondary pathway to anthracene. Overall, branching ratios of various $C_{14}H_{10}$ isomers produced through the primary and secondary reaction under the experimental conditions can be theoretically evaluated in a future work through kinetic modeling combined with computational fluid dynamics simulations of the gas flow in the reactor as outlined in a kinetic section in the Supplementary Materials, which also provides calculated rate constants for the prevailing reaction channels.

DISCUSSION

In summary, our combined experimental and computational investigation reveals the formation of phenanthrene and anthracene through distinct five-membered ring expansion mechanisms from the gas-phase radical-radical reaction of methyl ($CH_3^{\bullet}$) with resonance-stabilized fluorenyl ($C_{11}H_9^{\bullet}$), where products were detected isomer-selectively with the PEPICO technique using PIE curves and ms-TPE spectra. While the radical-radical recombination route to phenanthrene is expected, the pathway to anthracene via methyl attack on the opposing, low-spin-density side of fluorenyl should be negligible according to classical textbook knowledge. However, branching ratios to anthracene of over 10% even with the inclusion of additional isomers suggest that this mechanism may play a greater role in the PAH growth network present in extreme, high-temperature environments than anticipated, although the formation of anthracene may, in part, be attributed to the H-assisted isomerization of phenanthrene. Both phenanthrene and anthracene have been detected in carbonaceous chondrites such as Murchison (*25*) and Kolang (*47*) and were recently found in samples returned from the asteroid Ryugu (*27*), highlighting the interest in discovering alternate formation mechanisms for these PAHs from astrophysically relevant precursors. While the methyl radical was first detected in the ISM more than 20 years ago (*48*), fluorenyl has no explicit observation. However, as demonstrated in laminar flow combustion experiments—approximating conditions in circumstellar envelopes of carbon stars and planetary nebulae as their descendants—the fluorenyl radical can be produced at high temperatures from, e.g., ethylene and indene (*18*, *49*), both of which are prevalent in deep space (*30*, *31*, *50*), thus vouching for the feasibility of the title reaction in extraterrestrial environments.

Additionally, radical-radical reactions encompass a noteworthy role in the processes found in combustion systems (*39*). Specifically, conversion of five-membered to six-membered rings via ring expansion has previously been explored theoretically (*51*–*53*) and investigated with pyrolysis experiments (*54*–*58*). Our current study offers insight into bottom-up molecular mass growth processes of PAHs—which eventually lead to soot—through these radical-radical ring expansion mechanisms by revealing multiple pathways for fluorenyl conversion to phenanthrene and anthracene, in essence providing different ways for taking a multi-ringed aromatic species on track to grow into a three-dimensional carbonaceous nanostructure—due to five-membered rings instilling curvature in larger PAHs (*59*)—and converting it to a fully benzenoid PAH on the path to two-dimensional growth, inevitably changing the route toward soot formation. Overall, the use of tunable VUV light for isomer-selective exploration of PAH growth from resonance-stabilized hydrocarbon radicals enhances our fundamental understanding of interstellar carbon evolution, from small RSFRs such as propargyl up to carbonaceous nanoparticles and beyond.

MATERIALS AND METHODS

Experimental methods

The experiments were carried out at the Swiss Light Source (SLS) of the Paul Scherrer Institute (PSI) using the X04DB beamline. Measurements used a molecular beam apparatus coupled to a resistively heated silicon-carbide (SiC) chemical microreactor, which was operated with a double VMI photoelectron photoion coincidence spectrometer (*60*–*65*). Briefly, acetone [$CH_3C(O)CH_3$, 99%] was placed in a water–ice-cooled glass bubbler and seeded at 5% in helium (He, 99.996%, PanGas). The gas mixture was sent at a backing pressure of 150 torr and a flow rate of 80 sccm (standard cubic centimeters per minute) through a high-vacuum oven containing 9-bromofluorene ($C_{13}H_9Br$, 98%, Sigma-Aldrich), which was sublimed at 333 ± 1 K and incorporated into the gas flow, which exited the oven through a 200-μm-diameter nozzle into a SiC tube with 20-mm heated length and 1-mm inner diameter. Methyl (CH_3) and 9-fluorenyl ($C_{13}H_9$) radicals were generated in situ via pyrolysis of acetone and 9-bromofluorene, respectively, at a reactor temperature of 1700 ± 100 K measured by a type C thermocouple. Products formed attained supersonic expansion upon leaving the reactor and passed through a skimmer with a 2-mm-diameter orifice into the experimental chamber where the photoelectron photoion coincidence (PEPICO) spectrometer resides. Here, quasi-continuous synchrotron VUV radiation tuned from 7.00 to 9.00 eV is exploited to ionize reaction products under fragment-free soft ionization conditions (*66*, *67*). A constant electric field of 218 V cm^{-1} was used to extract both the cations and electrons in opposite directions to be velocity map imaged on separate position-sensitive delay-line anode detectors (Roentdek DLD40). Data obtained include PIE curves, which depict ion counts as a function of photon energy at a specific m/z, and ms-TPE spectra, which are collected from the same method as the PIE curves while selecting only the photoelectrons with kinetic energy less than 10 meV in coincidence with photoions at the desired m/z. The procedure of Sztáray and Baer (*68*) was used to subtract the hot electron signal from the threshold (kinetic energy less than 10 meV) electrons. Selecting only the room temperature background in the VMI for the ions results in a reduction in spectral broadening and hot bands from insufficient cooling of the molecular beam (*69*).

Computational methods

Ab initio G3(MP2,CC)//ωB97XD/6-311G(d,p) calculations have been used to optimize local minima and transition states on the $C_{14}H_{12}$ and $C_{14}H_{11}$ PESs accessed by the reaction of the fluorenyl and methyl radicals. The Cartesian coordinates (Å) and vibrational frequencies (cm^{-1}) for all species are reported in data S1. The G3(MP2,CC)//ωB97XD/6-311G(d,p) model chemistry scheme (*70*–*72*), which is expected to provide an accuracy of 4 to 8 kJ mol^{-1} for relative energies, involves geometry optimization and vibrational frequency calculations at the hybrid density functional ωB97XD/6-311G(d,p) level (*73*) followed by single-point energy refinement at the CCSD(T) (*74*, *75*)/6-311G(d,p) (*76*), MP2 (*77*)/6-311G(d,p), and MP2/G3Large (*67*) levels of theory aimed to evaluate the CCSD(T) energy with a large and flexible G3Large basis set. Zero-point vibrational energy corrections (ZPE) obtained at the ωB97XD/6-311G(d,p) level were also included. The absence of a meaningful multireference character in the wavefunctions was monitored using their T1 diagnostics (*78*, *79*), and no problematic cases were detected as T1 values did not exceed 0.015. The electronic structure calculations were carried out using the Gaussian 09 (*80*) and MOLPRO 2015 (*81*, *82*) program packages.

Possible assignments for $C_{14}H_{10}$ isomers were screened with an in-house code that retrieves compound information for a user-input chemical formula ($C_{14}H_{10}$) from the PubChem database (*83*) and generates Gaussian input files based on the InChI provided. Geometry optimization and frequency calculation for both neutral and cation was carried out at the B3LYP/CBSB7 level of theory. The zero-point corrected electronic energies were refined at CBS-QB3 (*84*) to calculate the AIEs using the Gaussian 16 Rev. C01 suite of programs (*85*). We calculated ionization energies of around 100 species, from which about 14 were in a ±0.1-eV energy range from the band at 7.60 eV. In addition, we applied a cutoff energy of 1.4 eV above phenanthrene, the most stable isomer, and ended up with five different isomers, for which we calculated the FC factors using eZspectrum (*86*). The resulting stick spectra were convoluted with Gaussian functions of 20- to 50-meV full width at half maximum and fitted to the experimental spectrum. Spectra of the five isomers of the $C_{14}H_{10}$ compositions along with FC simulations are depicted in fig. S5.

Supplementary Materials

The PDF file includes:

Supplementary Text
Figs. S1 to S6
Table S1
Legend for data S1
References

Other Supplementary Material for this manuscript includes the following:

Data S1

REFERENCES AND NOTES

1. I. Ratera, J. Veciana, Playing with organic radicals as building blocks for functional molecular materials. *Chem. Soc. Rev.* **41**, 303–349 (2012).
2. S. Sanvito, Molecular spintronics. *Chem. Soc. Rev.* **40**, 3336–3355 (2011).
3. T. Janoschka, M. D. Hager, U. S. Schubert, Powering up the future: Radical polymers for battery applications. *Adv. Mater.* **24**, 6397–6409 (2012).
4. D. Yuan, Y. Guo, Y. Zeng, Q. Fan, J. Wang, Y. Yi, X. Zhu, Air-stable n-type thermoelectric materials enabled by organic diradicaloids. *Angew. Chem. Int. Ed.* **58**, 4958–4962 (2019).
5. T. Minami, M. Nakano, Diradical character view of singlet fission. *J. Phys. Chem. Lett.* **3**, 145–150 (2012).
6. Q. Peng, A. Obolda, M. Zhang, F. Li, Organic light-emitting diodes using a neutral π radical as emitter: The emission from a doublet. *Angew. Chem. Int. Ed.* **54**, 7091–7095 (2015).
7. M. Agúndez, C. Cabezas, B. Tercero, N. Marcelino, J. D. Gallego, P. de Vicente, J. Cernicharo, Discovery of the propargyl radical (CH_2CCH) in TMC-1: One of the most abundant radicals ever found and a key species for cyclization to benzene in cold dark clouds. *Astron. Astrophys.* **647**, L10 (2021).
8. M. Agúndez, N. Marcelino, C. Cabezas, R. Fuentetaja, B. Tercero, P. de Vicente, J. Cernicharo, Detection of the propargyl radical at λ 3 mm. *Astron. Astrophys.* **657**, A96 (2022).
9. C. Cabezas, M. Agúndez, N. Marcelino, B. Tercero, J. R. Pardo, P. de Vicente, J. Cernicharo, Discovery of interstellar 3-cyano propargyl radical, CH_2CCCN. *Astron. Astrophys.* **654**, L9 (2021).
10. P. Thaddeus, C. Gottlieb, A. Hjalmarson, L. Johansson, W. Irvine, P. Friberg, R. Linke, Astronomical identification of the C_3H radical. *Astrophys. J.* **294**, L49 (1985).
11. J. Cernicharo, C. Kahane, J. Gomez-Gonzalez, M. Guélin, Tentative detection of the C_5H radical. *Astron. Astrophys.* **164**, L1 (1986).
12. W. M. Irvine, P. Friberg, A. Hjalmarson, S. Ishikawa, N. Kaifu, K. Kawaguchi, S. Madden, H. Matthews, M. Ohishi, S. Saito, H. Suzuki, P. Thaddeus, B. E. Turner, S. Yamamoto, L. M. Ziurys, Identification of the interstellar cyanomethyl radical (CH_2CN) in the molecular clouds TMC-1 and Sagittarius B2. *Astrophys. J.* **334**, L107 (1988).
13. J. Cernicharo, M. Guélin, J. R. Pardo, Detection of the linear radical HC_4N in IRC +10216. *Astrophys. J.* **615**, L145–L148 (2004).
14. J. Cernicharo, M. Agúndez, C. Cabezas, B. Tercero, N. Marcelino, R. Fuentetaja, J. R. Pardo, P. de Vicente, Discovery of HCCCO and C_5O in TMC-1 with the QUIJOTE line survey. *Astron. Astrophys.* **656**, L21 (2021).
15. K. O. Johansson, M. P. Head-Gordon, P. E. Schrader, K. R. Wilson, H. A. Michelsen, Resonance-stabilized hydrocarbon-radical chain reactions may explain soot inception and growth. *Science* **361**, 997–1000 (2018).
16. S. Sinha, R. K. Rahman, A. Raj, On the role of resonantly stabilized radicals in polycyclic aromatic hydrocarbon (PAH) formation: Pyrene and fluoranthene formation from benzyl–Indenyl addition. *Phys. Chem. Chem. Phys.* **19**, 19262–19278 (2017).
17. D. E. Couch, A. J. Zhang, C. A. Taatjes, N. Hansen, Experimental observation of hydrocarbon growth by resonance-stabilized radical–Radical chain reaction. *Angew. Chem. Int. Ed.* **60**, 27230–27235 (2021).
18. J. A. Rundel, C. M. Thomas, P. E. Schrader, K. R. Wilson, K. O. Johansson, R. P. Bambha, H. A. Michelsen, Promotion of particle formation by resonance-stabilized radicals during hydrocarbon pyrolysis. *Combust. Flame* **243**, 111942 (2022).
19. C. Y. Wang, L. Zhao, R. I. Kaiser, Gas-phase preparation of the 14π Hückel polycyclic aromatic anthracene and phenanthrene isomers ($C_{14}H_{10}$) via the Propargyl Addition–BenzAnnulation (PABA) mechanism. *ChemPhysChem* **25**, e202400151 (2024).
20. A. G. G. M. Tielens, Interstellar polycyclic aromatic hydrocarbon molecules. *Annu. Rev. Astron. Astrophys.* **46**, 289–337 (2008).
21. B. A. McGuire, R. A. Loomis, A. M. Burkhardt, K. L. K. Lee, C. N. Shingledecker, S. B. Charnley, I. R. Cooke, M. A. Cordiner, E. Herbst, S. Kalenskii, M. A. Siebert, E. R. Willis, C. Xue, A. J. Remijan, M. C. McCarthy, Detection of two interstellar polycyclic aromatic hydrocarbons via spectral matched filtering. *Science* **371**, 1265–1269 (2021).
22. M. L. Sita, P. B. Changala, C. Xue, A. M. Burkhardt, C. N. Shingledecker, K. L. K. Lee, R. A. Loomis, E. Momjian, M. A. Siebert, D. Gupta, E. Herbst, A. J. Remijan, M. C. McCarthy, I. R. Cooke, B. A. McGuire, Discovery of interstellar 2-cyanoindene (2-C_9H_7CN) in GOTHAM observations of TMC-1. *Astrophys. J. Lett.* **938**, L12 (2022).
23. D. Loru, C. Cabezas, J. Cernicharo, M. Schnell, A. L. Steber, Detection of ethynylbenzene in TMC-1 and the interstellar search for 1,2-diethynylbenzene. *Astron. Astrophys.* **677**, A166 (2023).
24. L. Becker, T. E. Bunch, Fullerenes, fulleranes and polycyclic aromatic hydrocarbons in the Allende meteorite. *Meteorit. Planet. Sci.* **32**, 479–487 (1997).
25. B. P. Basile, B. S. Middleditch, J. Oró, Polycyclic aromatic hydrocarbons in the Murchison meteorite. *Org. Geochem.* **5**, 211–216 (1984).
26. T. J. Wdowiak, G. C. Flickinger, J. R. Cronin, Insoluble organic material of the Orgueil carbonaceous chondrite and the unidentified infrared bands. *Astrophys. J.* **328**, L75–L79 (1988).
27. S. S. Zeichner, J. C. Aponte, S. Bhattacharjee, G. Dong, A. E. Hofmann, J. P. Dworkin, D. P. Glavin, J. E. Elsila, H. V. Graham, H. Naraoka, Y. Takano, S. Tachibana, A. T. Karp, K. Grice, A. I. Holman, K. H. Freeman, H. Yurimoto, T. Nakamura, T. Noguchi, R. Okazaki, H. Yabuta, K. Sakamoto, T. Yada, M. Nishimura, A. Nakato, A. Miyazaki, K. Yogata, M. Abe, T. Okada, T. Usui, M. Yoshikawa, T. Saiki, S. Tanaka, F. Terui, S. Nakazawa, S.-i. Watanabe, Y. Tsuda, K. Hamase, K. Fukushima, D. Aoki, M. Hashiguchi, H. Mita, Y. Chikaraishi, N. Ohkouchi, N. O. Ogawa, S. Sakai, E. T. Parker, H. L. McLain, F.-R. Orthous-Daunay, V. Vuitton, C. Wolters, P. Schmitt-Kopplin, N. Hertkorn, R. Thissen, A. Ruf, J. Isa, Y. Oba, T. Koga, T. Yoshimura, D. Araoka, H. Sugahara, A. Furusho, Y. Furukawa, J. Aoki, K. Kano, S.-i. M. Nomura, K. Sasaki, H. Sato, T. Yoshikawa, S. Tanaka, M. Morita, M. Onose, F. Kabashima, K. Fujishima, T. Yamazaki, Y. Kimura, J. M. Eiler, Polycyclic aromatic hydrocarbons in samples of Ryugu formed in the interstellar medium. *Science* **382**, 1411–1416 (2023).
28. G. Wenzel, I. R. Cooke, P. B. Changala, E. A. Bergin, S. Zhang, A. M. Burkhardt, A. N. Byrne, S. B. Charnley, M. A. Cordiner, M. Duffy, Z. T. P. Fried, H. Gupta, M. S. Holdren, A. Lipnicky, R. A. Loomis, H. T. Shay, C. N. Shingledecker, M. A. Siebert, D. A. Stewart, R. H. J. Willis, C. Xue, A. J. Remijan, A. E. Wendlandt, M. C. McCarthy, B. A. McGuire, Detection of interstellar 1-cyanopyrene: A four-ring polycyclic aromatic hydrocarbon. *Science* **386**, 810–813 (2024).
29. G. Wenzel, T. H. Speak, P. B. Changala, R. H. J. Willis, A. M. Burkhardt, S. Zhang, E. A. Bergin, A. N. Byrne, S. B. Charnley, Z. T. P. Fried, H. Gupta, E. Herbst, M. S. Holdren, A. Lipnicky, R. A. Loomis, C. N. Shingledecker, C. Xue, A. J. Remijan, A. E. Wendlandt, M. C. McCarthy, I. R. Cooke, B. A. McGuire, Detections of interstellar aromatic nitriles 2-cyanopyrene and 4-cyanopyrene in TMC-1. *Nat. Astron.* **9**, 262 (2025).
30. J. Cernicharo, M. Agúndez, C. Cabezas, B. Tercero, N. Marcelino, J. R. Pardo, P. de Vicente, Pure hydrocarbon cycles in TMC-1: Discovery of ethynyl cyclopropenylidene, cyclopentadiene, and indene. *Astron. Astrophys.* **649**, L15 (2021).
31. A. M. Burkhardt, K. L. K. Lee, P. B. Changala, C. N. Shingledecker, I. R. Cooke, R. A. Loomis, H. Wei, S. B. Charnley, E. Herbst, M. C. McCarthy, B. A. McGuire, Discovery of the pure polycyclic aromatic hydrocarbon indene (c-C_9H_8) with GOTHAM observations of TMC-1. *Astrophys. J. Lett.* **913**, L18 (2021).
32. J. Cernicharo, C. Cabezas, R. Fuentetaja, M. Agúndez, B. Tercero, J. Janeiro, M. Juanes, R. I. Kaiser, Y. Endo, A. L. Steber, D. Pérez, C. Pérez, A. Lesarri, N. Marcelino, P. de Vicente, Discovery of two cyano derivatives of acenaphthylene ($C_{12}H_8$) in TMC-1 with the QUIJOTE line survey. *Astron. Astrophys.* **690**, L13 (2024).
33. N. Balucani, O. Asvany, A. H. H. Chang, S. H. Lin, Y. T. Lee, R. I. Kaiser, H. F. Bettinger, P. V. R. Schleyer, H. F. Schaefer III, Crossed beam reaction of cyano radicals with hydrocarbon molecules. I. Chemical dynamics of cyanobenzene (C_6H_5CN; X^1A_1) and perdeutero cyanobenzene (C_6D_5CN; X^1A_1) formation from reaction of CN($X^2\Sigma^+$) with benzene $C_6H_6(X^1A_{1g})$, and d_6-benzene $C_6D_6(X^1A_{1g})$. *J. Chem. Phys.* **111**, 7457–7471 (1999).
34. N. Balucani, O. Asvany, L. C. L. Huang, Y. T. Lee, R. I. Kaiser, Y. Osamura, H. F. Bettinger, Formation of nitriles in the interstellar medium via reactions of cyano radicals, CN($X^2\Sigma^+$), with unsaturated hydrocarbons. *Astrophys. J.* **545**, 892–906 (2000).
35. Z. Yang, I. A. Medvedkov, S. J. Goettl, A. A. Nikolayev, A. M. Mebel, X. Li, R. I. Kaiser, Low-temperature gas-phase formation of cyclopentadiene and its role in the formation of aromatics in the interstellar medium. *Proc. Natl. Acad. Sci. U.S.A.* **121**, e2409933121 (2024).
36. E. R. Micelotta, A. P. Jones, A. G. G. M. Tielens, Polycyclic aromatic hydrocarbon processing in interstellar shocks. *Astron. Astrophys.* **510**, A36 (2010).
37. E. R. Micelotta, A. P. Jones, A. G. G. M. Tielens, Polycyclic aromatic hydrocarbon processing in a hot gas. *Astron. Astrophys.* **510**, A37 (2010).
38. E. R. Micelotta, A. P. Jones, A. G. G. M. Tielens, Polycyclic aromatic hydrocarbon processing by cosmic rays. *Astron. Astrophys.* **526**, A52 (2011).
39. E. Reizer, B. Viskolcz, B. Fiser, Formation and growth mechanisms of polycyclic aromatic hydrocarbons: A mini-review. *Chemosphere* **291**, 132793 (2022).
40. M. Frenklach, A. W. Jasper, A. M. Mebel, Phenalenyl growth reactions and implications for prenucleation chemistry of aromatics in flames. *Phys. Chem. Chem. Phys.* **26**, 13034–13048 (2024).
41. P. M. Mayer, V. Blanchet, C. Joblin, Threshold photoelectron study of naphthalene, anthracene, pyrene, 1,2-dihydronaphthalene, and 9,10-dihydroanthracene. *J. Chem. Phys.* **134**, 244312 (2011).
42. G. Rouillé, S. A. Krasnokutski, D. Fulvio, C. Jäger, T. Henning, G. A. Garcia, X. F. Tang, L. Nahon, Dissociative photoionization of polycyclic aromatic hydrocarbon molecules carrying an ethynyl group. *Astrophys. J.* **810**, 114 (2015).
43. Y. Li, J. Yang, Z. Cheng, Photoionization Cross Section Database, Version 2.0 (National Synchrotron Radiation Laboratory, 2017); http://flame.nsrl.ustc.edu.cn/database/data.php.
44. T. Sattasathuchana, J. S. Siegel, K. K. Baldridge, Generalized analytic approach for determination of multidimensional Franck–Condon factors: Simulated photoelectron spectra of polynuclear aromatic hydrocarbons. *J. Chem. Theory Comput.* **16**, 4521–4532 (2020).
45. Y. Tian, K. Uchida, H. Kurata, Y. Hirao, T. Nishiuchi, T. Kubo, Design and synthesis of new stable fluorenyl-based radicals. *J. Am. Chem. Soc.* **136**, 12784–12793 (2014).

46. L. Zhao, R. I. Kaiser, B. Xu, U. Ablikim, M. Ahmed, M. M. Evseev, E. K. Bashkirov, V. N. Azyazov, A. M. Mebel, Low-temperature formation of polycyclic aromatic hydrocarbons in Titan's atmosphere. *Nat. Astron.* **2**, 973–979 (2018).
47. M. Lecasble, L. Remusat, J.-C. Viennet, B. Laurent, S. Bernard, Polycyclic aromatic hydrocarbons in carbonaceous chondrites can be used as tracers of both pre-accretion and secondary processes. *Geochim. Cosmochim. Acta* **335**, 243–255 (2022).
48. H. Feuchtgruber, F. P. Helmich, E. F. van Dishoeck, C. M. Wright, Detection of interstellar CH_3. *Astrophys. J.* **535**, L111 (2000).
49. H. Jin, L. Xing, J. Hao, J. Yang, Y. Zhang, C. Cao, Y. Pan, A. Farooq, A chemical kinetic modeling study of indene pyrolysis. *Combust. Flame* **206**, 1–20 (2019).
50. A. L. Betz, Ethylene in IRC +10216. *Astrophys. J.* **244**, L103 (1981).
51. C. F. Melius, M. E. Colvin, N. M. Marinov, W. J. Pit, S. M. Senkan, Reaction mechanisms in aromatic hydrocarbon formation involving the C_5H_5 cyclopentadienyl moiety. *Symp. (Int.) Combust.* **26**, 685 (1996).
52. A. W. Jasper, N. Hansen, Hydrogen-assisted isomerizations of fulvene to benzene and of larger cyclic aromatic hydrocarbons. *Proc. Combust. Inst.* **34**, 279–287 (2013).
53. C. Cavallotti, D. Polino, On the kinetics of the C_5H_5+C_5H_5 reaction. *Proc. Combust. Inst.* **34**, 557–564 (2013).
54. C. S. McEnally, L. D. Pfefferle, An experimental study in non-premixed flames of hydrocarbon growth processes that involve five-membered carbon rings. *Combust. Sci. Technol.* **131**, 323–344 (1998).
55. R. P. Lindstedt, K. A. Rizos, The formation and oxidation of aromatics in cyclopentene and methyl-cyclopentadiene mixtures. *Proc. Combust. Inst.* **29**, 2291–2298 (2002).
56. J. Filley, J. T. McKinnon, Dimerization of cyclopentadienyl radical to produce naphthalene. *Combust. Flame* **124**, 721–723 (2001).
57. L. Zhao, R. Kaiser, W. Lu, B. Xu, M. Ahmed, A. N. Morozov, A. M. Mebel, A. H. Howlader, S. F. Wnuk, Molecular mass growth through ring expansion in polycyclic aromatic hydrocarbons via radical–radical reactions. *Nat. Commun.* **10**, 3689 (2019).
58. R. I. Kaiser, L. Zhao, W. Lu, M. Ahmed, M. V. Zagidullin, V. N. Azyazov, A. M. Mebel, Formation of benzene and naphthalene through cyclopentadienyl-mediated radical–radical reactions. *J. Phys. Chem. Lett.* **13**, 208–213 (2022).
59. J. W. Martin, K. Bowal, A. Menon, R. I. Slavchov, J. Akroyd, S. Mosbach, M. Kraft, Polar curved polycyclic aromatic hydrocarbons in soot formation. *Proc. Combust. Inst.* **37**, 1117–1123 (2019).
60. A. Bodi, M. Johnson, T. Gerber, Z. Gengeliczki, B. Sztáray, T. Baer, Imaging photoelectron photoion coincidence spectroscopy with velocity focusing electron optics. *Rev. Sci. Instrum.* **80**, 034101 (2009).
61. M. Johnson, A. Bodi, L. Schulz, T. Gerber, Vacuum ultraviolet beamline at the Swiss Light Source for chemical dynamics studies. *Nucl. Instr. Meth. Phys. Res. Sect. A* **610**, 597–603 (2009).
62. J. Bouwman, A. Bodi, P. Hemberger, Nitrogen matters: The difference between PANH and PAH formation. *Phys. Chem. Chem. Phys.* **20**, 29910–29917 (2018).
63. P. Hemberger, J. A. van Bokhoven, J. Pérez-Ramírez, A. Bodi, New analytical tools for advanced mechanistic studies in catalysis: Photoionization and photoelectron photoion coincidence spectroscopy. *Cat. Sci. Technol.* **10**, 1975–1990 (2020).
64. E. Mendez-Vega, W. Sander, P. Hemberger, Isomer-selective threshold photoelectron spectra of phenylnitrene and its thermal rearrangement products. *J. Phys. Chem. A* **124**, 3836–3843 (2020).
65. S. Grimm, S.-J. Baik, P. Hemberger, A. Bodi, A. M. Kempf, T. Kasper, B. Atakan, Gas-phase aluminium acetylacetonate decomposition: revision of the current mechanism by VUV synchrotron radiation. *Phys. Chem. Chem. Phys.* **23**, 15059–15075 (2021).
66. F. Qi, Combustion chemistry probed by synchrotron VUV photoionization mass spectrometry. *Proc. Combust. Inst.* **34**, 33–63 (2013).
67. T. A. Cool, A. McIlroy, F. Qi, P. R. Westmoreland, L. Poisson, D. S. Peterka, M. Ahmed, Photoionization mass spectrometer for studies of flame chemistry with a synchrotron light source. *Rev. Sci. Instrum.* **76**, 094102 (2005).
68. B. Sztáray, T. Baer, Suppression of hot electrons in threshold photoelectron photoion coincidence spectroscopy using velocity focusing optics. *Rev. Sci. Instrum.* **74**, 3763–3768 (2003).
69. P. Hemberger, X. Wu, Z. Pan, A. Bodi, Continuous pyrolysis microreactors: Hot sources with little cooling? New insights utilizing cation velocity map imaging and threshold photoelectron spectroscopy. *J. Phys. Chem. A* **126**, 2196–2210 (2022).
70. A. G. Baboul, L. A. Curtiss, P. C. Redfern, K. Raghavachari, Gaussian-3 theory using density functional geometries and zero-point energies. *J. Chem. Phys.* **110**, 7650–7657 (1999).
71. L. A. Curtiss, K. Raghavachari, P. C. Redfern, A. G. Baboul, J. A. Pople, Gaussian-3 theory using coupled cluster energies. *Chem. Phys. Lett.* **314**, 101–107 (1999).
72. L. A. Curtiss, K. Raghavachari, P. C. Redfern, V. Rassolov, J. A. Pople, Gaussian-3 (G3) theory for molecules containing first and second-row atoms. *J. Chem. Phys.* **109**, 7764–7776 (1998).
73. J.-D. Chai, M. Head-Gordon, Long-range corrected hybrid density functionals with damped atom–atom dispersion corrections. *Phys. Chem. Chem. Phys.* **10**, 6615–6620 (2008).
74. R. J. Bartlett, G. D. Purvis, Many-body perturbation theory, coupled-pair many-electron theory, and the importance of quadruple excitations for the correlation problem. *Int. J. Quantum Chem.* **14**, 561–581 (1978).
75. J. A. Pople, M. Head-Gordon, K. Raghavachari, Quadratic configuration interaction. A general technique for determining electron correlation energies. *J. Chem. Phys.* **87**, 5968–5975 (1987).
76. R. Krishnan, J. S. Binkley, R. Seeger, J. A. Pople, Self-consistent molecular orbital methods. XX. A basis set for correlated wave functions. *J. Chem. Phys.* **72**, 650–654 (1980).
77. M. J. Frisch, M. Head-Gordon, J. A. Pople, A direct MP2 gradient method. *Chem. Phys. Lett.* **166**, 275–280 (1990).
78. T. J. Lee, J. E. Rice, G. E. Scuseria, H. F. Schaefer, Theoretical investigations of molecules composed only of fluorine, oxygen and nitrogen: Determination of the equilibrium structures of FOOF, $(NO)_2$ and FNNF and the transition state structure for FNNF *cis-trans* isomerization. *Theor. Chim. Acta* **75**, 81–98 (1989).
79. T. J. Lee, Comparison of the T_1 and D_1 diagnostics for electronic structure theory: A new definition for the open-shell D_1 diagnostic. *Chem. Phys. Lett.* **372**, 362–367 (2003).
80. M. J. Frisch, G. W. Trucks, H. B. Schlegel, G. E. Scuseria, M. A. Robb, J. R. Cheeseman, G. Scalmani, V. Barone, B. Mennucci, G. A. Petersson, H. Nakatsuji, M. Caricato, X. Li, H. P. Hratchian, A. F. Izmaylov, J. Bloino, G. Zheng, J. L. Sonnenberg, M. Hada, M. Ehara, K. Toyota, R. Fukuda, J. Hasegawa, M. Ishida, T. Nakajima, Y. Honda, O. Kitao, H. Nakai, T. Vreven, J. Montgomery, J A, J. E. Peralta, F. Ogliaro, M. Bearpark, J. J. Heyd, E. Brothers, K. N. Kudin, V. N. Staroverov, R. Kobayashi, J. Normand, K. Raghavachari, A. Rendell, J. C. Burant, S. S. Iyengar, J. Tomasi, M. Cossi, N. Rega, J. M. Millam, M. Klene, J. E. Knox, J. B. Cross, V. Bakken, C. Adamo, J. Jaramillo, R. Gomperts, R. E. Stratmann, O. Yazyev, A. J. Austin, R. Cammi, C. Pomelli, J. W. Ochterski, R. L. Martin, K. Morokuma, V. G. Zakrzewski, G. A. Voth, P. Salvador, J. J. Dannenberg, S. Dapprich, A. D. Daniels, Ö. Farkas, J. B. Foresman, J. V. Ortiz, J. Cioslowski, D. J. Fox, *Gaussian 09, Revision A.02* (Gaussian Inc., 2009); http://www.gaussian.com.
81. H. J. Werner, P. J. Knowles, G. Knizia, F. R. Manby, M. Schütz, P. Celani, W. Györffy, D. Kats, T. Korona, R. Lindh, A. Mitrushenkov, G. Rauhut, K. R. Shamasundar, T. B. Adler, R. D. Amos, A. Bernhardsson, A. Berning, D. L. Cooper, J. O. Deegan, A. J. Dobbyn, F. Eckert, E. Goll, C. Hampel, A. Hesselmann, G. Hetzer, T. Hrenar, G. Jansen, C. Köppl, Y. Liu, A. W. Lloyd, R. A. Mata, A. J. May, S. J. McNicholas, W. Meyer, M. E. Mura, A. Nicklass, D. P. O'Neill, P. Palmieri, D. Peng, K. Pflüger, R. Pitzer, M. Reiher, T. Shiozaki, H. Stoll, A. J. Stone, R. Tarroni, T. Thorsteinsson, M. Wang, *MOLPRO, a Package of Ab Initio Programs, Version 2015.2* (University of Cardiff, 2015); http://www.molpro.net.
82. H.-J. Werner, P. J. Knowles, G. Knizia, F. R. Manby, M. Schütz, Molpro: A general-purpose quantum chemistry program package. *WIREs Comput. Mol. Sci.* **2**, 242–253 (2012).
83. S. Kim, J. Chen, T. Cheng, A. Gindulyte, J. He, S. He, Q. Li, B. A. Shoemaker, P. A. Thiessen, B. Yu, L. Zaslavsky, J. Zhang, E. E. Bolton, PubChem 2025 update. *Nucleic Acids Res.* **53**, D1516–D1525 (2024).
84. J. A. Montgomery Jr., M. J. Frisch, J. W. Ochterski, G. A. Petersson, A complete basis set model chemistry. VII. Use of the minimum population localization method. *J. Chem. Phys.* **112**, 6532–6542 (2000).
85. M. J. Frisch, G. W. Trucks, H. B. Schlegel, G. E. Scuseria, M. A. Robb, J. R. Cheeseman, G. Scalmani, V. Barone, G. A. Petersson, H. Nakatsuji, X. Li, M. Caricato, A. V. Marenich, J. Bloino, B. G. Janesko, R. Gomperts, B. Mennucci, H. P. Hratchian, J. V. Ortiz, A. F. Izmaylov, J. L. Sonnenberg, Williams, Williams, F. Ding, F. Lipparini, F. Egidi, J. Goings, B. Peng, A. Petrone, T. Henderson, D. Ranasinghe, V. G. Zakrzewski, J. Gao, N. Rega, G. Zheng, W. Liang, M. Hada, M. Ehara, K. Toyota, R. Fukuda, J. Hasegawa, M. Ishida, T. Nakajima, Y. Honda, O. Kitao, H. Nakai, T. Vreven, K. Throssell, J. A. Montgomery Jr, J. E. Peralta, F. Ogliaro, M. J. Bearpark, J. J. Heyd, E. N. Brothers, K. N. Kudin, V. N. Staroverov, T. A. Keith, R. Kobayashi, J. Normand, K. Raghavachari, A. P. Rendell, J. C. Burant, S. S. Iyengar, J. Tomasi, M. Cossi, J. M. Millam, M. Klene, C. Adamo, R. Cammi, J. W. Ochterski, R. L. Martin, K. Morokuma, O. Farkas, J. B. Foresman, D. J. Fox, *Gaussian 16, Revision C.01* (Gaussian Inc., 2016); http://www.gaussian.com.
86. S. Gozem, A. I. Krylov, The ezSpectra suite: An easy-to-use toolkit for spectroscopy modeling. *WIREs Comput. Mol. Sci.* **12**, e1546 (2022).
87. Y. Georgievskii, J. A. Miller, M. P. Burke, S. J. Klippenstein, Reformulation and solution of the master equation for multiple-well chemical reactions. *J. Phys. Chem. A* **117**, 12146–12154 (2013).
88. S. J. Klippenstein, J. I. Cline, Classical phase space theory for product state distributions with application to the *v–j* vector correlation. *J. Chem. Phys.* **103**, 5451–5460 (1995).
89. Y. Georgievskii, S. J. Klippenstein, Master Equation System Solver [MESS], 2016.3.23 (2015); https://tcg.cse.anl.gov/papr.
90. J. P. Maier, D. W. Turner, Steric inhibition of resonance studied by molecular photoelectron spectroscopy. Part 1—Biphenyls. *Faraday Discuss. Chem. Soc.* **54**, 149–167 (1972).
91. L. Crisci, S. Di Grande, C. Cavallotti, V. Barone, Toward an accurate black-box tool for the kinetics of gas-phase reactions involving barrier-less elementary steps. *J. Chem. Theory Comput.* **19**, 7626–7639 (2023).

92. J. F. Alarcon, A. N. Morozov, A. M. Mebel, A. Della Libera, L. Pratali Maffei, C. Cavallotti, Mechanism and kinetics of the oxidation of propargyl radical by atomic oxygen. *Proc. Combust. Inst.* **40**, 105372 (2024).

Acknowledgments

The PEPICO measurements were performed at the VUV (x04db) beamline of the Swiss Light Source, located at the Paul Scherrer Institute, Villigen, Switzerland. Funding: The experimental studies at the University of Hawaii were supported by the US Department of Energy, Basic Energy Sciences DE-FG02-03ER15411. **Author contributions:** R.I.K. designed research. S.J.G. and A.M.T. performed experiments. V.S.K., V.N.A., K.K., P.H., and A.M.M. performed calculations. S.J.G., P.H., A.M.M., and R.I.K. analyzed data. S.J.G., P.H., A.M.M., and R.I.K. wrote the paper. The manuscript was read, revised, and approved by all coauthors. **Competing interests:** The authors declare that they have no competing interests. **Data and materials availability:** All data needed to evaluate the conclusions in the paper are present in the paper and/or the Supplementary Materials.

Submitted 3 December 2024
Accepted 2 May 2025
Published 6 June 2025
10.1126/sciadv.adv0692